Available online at www.sciencedirect.com

jmr&t Journal of Materials Research and Technology

journal homepage: www.elsevier.com/locate/jmrt

Original Article

Multiaxial fatigue life estimation based on weight-averaged maximum damage plane under variable amplitude loading

Zhi-Qiang Tao [a,b,c], Guian Qian [b,c,*], Xiang Li [d], Jingyu Sun [b,c], Zi-Ling Zhang [e], Dao-Hang Li [f]

[a] College of Robotics, Beijing Union University, Beijing, 100020, China
[b] State Key Laboratory of Nonlinear Mechanics (LNM), Institute of Mechanics, Chinese Academy of Sciences, Beijing, 100190, China
[c] School of Engineering Science, University of Chinese Academy of Sciences, Beijing, 100049, China
[d] China Special Equipment Inspection and Research Institute, Beijing, 100029, China
[e] Logistics Engineering College, Shanghai Maritime University, Shanghai, 201306, China
[f] Faculty of Materials and Manufacturing, Beijing University of Technology, Beijing, 100124, China

ARTICLE INFO

Article history:
Received 27 October 2022
Accepted 27 January 2023
Available online 2 February 2023

Keywords:
Multiaxial fatigue
Lifetime estimation
Weight function
Critical plane
Variable amplitude loading

ABSTRACT

An innovative critical plane determination approach with weight-averaged largest fatigue damage is proposed, in which the material failure modes can be considered. If material exhibits shear cracking behavior, a strain-based critical plane model with shear failure mode is selected to evaluate the weight function. Otherwise, other one with tensile failure mode is adopted. According to the proposed critical plane, a multiaxial fatigue lifetime estimation methodology is established for evaluating fatigue life. And, six kinds of materials are employed to validate the validity of presented methodology. The validation results reveal the presented methodology can estimate the orientation angles of failure plane accurately and supply satisfactory fatigue lifetime estimations for both shear and tensile failure mode materials. Furthermore, the proposed critical plane framework can be extended to be utilized with stress-based fatigue criteria, and prediction results show a good agreement with experimental data by another two materials.

1. Introduction

Engineering components and mechanical parts, such as pressure containers, crankshafts, turbine rotors, automobile engines, always suffer from multiaxial variable amplitude loadings [1–4]. For these mechanical components, one of the major failure causes is multiaxial fatigue failure. During the past few decades, researchers have paid considered attention to multiaxial fatigue life estimation of mechanical components. However, due to sophisticated mechanisms of fatigue crack initiation and propagation, multiaxial fatigue lifetime

* Corresponding author.
E-mail address: qianguian@imech.ac.cn (G. Qian).
https://doi.org/10.1016/j.jmrt.2023.01.196

Nomenclature

C	safety coefficient changing between 0 and 1
f_{-1}	fatigue limit for bending loadings
τ_{-1}	torsional fatigue limit
b	axial fatigue strength exponent
b_0	shear fatigue strength exponent
c	axial fatigue ductility exponent
c_0	shear fatigue ductility exponent
E	modulus of elasticity
G	shear modulus
K	material constant in the FS parameter
M	transformation matrix
ε	axial strain
ε'_f	axial fatigue ductility coefficient
γ	shear strain
$\Delta\gamma$	shear strain range
γ'_f	shear fatigue ductility coefficient
σ	axial stress
σ_n	normal stress on the maximum shear plane
σ_y	yield stress
σ'_f	axial fatigue strength coefficient
τ	shear stress
τ'_f	shear fatigue strength coefficient
υ_e	elastic Poisson's ratio
υ_{eff}	effective Poisson's ratio
D	fatigue damage
t	time
$\sigma_1(t)$	largest principal stress at time point t
ε_{eq}	von Mises equivalent strain
σ_{eq}	von Mises equivalent stress
WB	Wang and Brown
VF	Varvani-Farahani
FS	Fatemi and Socie
SWT	Smith-Watson-Topper

Subscripts

cr	critical plane
max	maximum value
n	normal direction

estimation is still considered as a particularly tricky question under variable amplitude loadings [5–8]. In order to ensure long-term safety and stability, additional research efforts are needed for effective multiaxial fatigue life prediction approaches of mechanical components.

The critical plane method has an explicit physical meaning, which is known as a reasoned method and is widely used within multiaxial fatigue lifetime estimation. Many approaches have been presented to calculate the critical plane for multiaxial constant amplitude loadings. For instance, for purpose of conducting the multiaxial fatigue estimation of some metals with tensile failure mode, Socie and cooperators [9–11] reconstructed the Smith-Watson-Topper damage parameter [12] and considered the critical plane as the largest normal strain amplitude plane. Socie and Fatemi [13] proposed the material plane experiencing the largest shear strain range as the critical plane, the initiation and initial propagation of fatigue cracks takes place upon the critical plane. Within the FS fatigue damage model, the influence of normal stress upon the critical plane was considered using the largest normal stress term. Wang and Brown [14] defined the maximum shear strain amplitude plane as the critical plane. In the WB damage parameter, initial fatigue crack propagation was dominated via the largest shear strain range, and the secondary important influence factor was considered as the normal strain excursion during one reversal of the largest shear strain. According to the various sorts of researched materials, selected loading modes and imposed strain amplitudes, Socie [10] presented the maximum shear or normal strain range plane as the critical plane, the normal strains and stresses upon the critical plane are able to assist in the fatigue rupture. Varvani-Farahani and his research group [15–17] considered the critical plane as the plane undergoing the maximum shear stress and strain Mohr's circles through a cycle. The calculated shear and normal strain energy is summed up upon the critical plane within the VF fatigue damage model. The critical plane in Varvani's damage model was taken as a plane to maximize product of shear and tensile strain energies over loading cycles. A comprehensive review of this model was done by researchers in [18]. In addition, many fatigue lifetime estimation approaches have been proposed on account of the critical plane [19].

The largest shear planes with respect to the different counted cycles are always changing under multiaxial variable amplitude out-of-phase loadings [19]. With regard to variable amplitude multiaxial loadings, lots of researchers have presented various approaches for the purpose of determining the critical plane direction. These approaches are able to be primarily divided into four types [20], those are, the variance approach [21], the weight function approach [22], the damage accumulation approach [23,24] and the energy based-critical plane approach [5,11,15–17].

In order to relate the direction of the largest shear strain plane at every instant with the direction of finial critical plane, Wang and Wang [25] employed the approach of weight function. The direction angle $\overline{\theta}$ of critical plane determined by the weight-averaged function is able to be shown as follow:

$$\overline{\theta} = \frac{1}{\sum_{i=1}^{n} w(t_i)} \sum_{i=1}^{n} \theta(t_i) w(t_i) \tag{1}$$

where $\theta(t_i)$ is the direction angle of largest shear strain plane with respect to time point t_i. n is the counted number of time instants. $w(t_i)$ is the weight function with respect to the largest shear strain plane, which can be determined utilizing the mathematical equation as follow:

$$w(t_i) = \begin{cases} D_i & \gamma_{\max}(t_i) \geq \dfrac{\tau_{-1}}{G} \\ 0 & \gamma_{\max}(t_i) < \dfrac{\tau_{-1}}{G} \end{cases} \tag{2}$$

where τ_{-1} is the torsional fatigue limit, D_i is the fatigue damage with respect to the largest shear strain, and G is the shear modulus.

By making an average of the instantaneous values of three Euler angles, Carpinteri et al. [26] presented the weighted mean

principal stress directions to calculate the direction angle of critical plane. Furthermore, Carpinteri and Spagnoli [27] proposed a weight function to calculate the orientation angle of mean principal stress, which can be denoted as follow:

$$w(k)=\begin{cases} 0 & if\ \sigma_1(t)<Cf_{-1} \\ \left(\frac{\sigma_1(t)}{f_{-1}}\right)^{m_\sigma} & if\ \sigma_1(t)<Cf_{-1} \end{cases} \quad 0<\ C\leq 1 \tag{3}$$

where $\sigma_1(t)$ is the largest principal stress at time point t, f_{-1} is the limit of fatigue for bending loadings, C is a safety coefficient changing between 0 and 1, exponent $m_\sigma=-1/m$ can be dependent upon the negative slope m of S–N curve.

For the entire loading history, Shamsaei et al. [24,28] mentioned that the critical plane cannot be computed utilizing the Wang-Brown reversal count approach. On the basis of the Wang-Brown reversal counting approach, the critical planes can be different for all counted reversals. However, fatigue damage with regard to the different critical planes is accumulated for all counted reversals. Furthermore, Shamsaei et al. [23] compute the fatigue damage for each segment of loading history, which is determined by employing FS damage model upon every candidate plane with orientation angle $0^\circ \leq \theta<180^\circ$. Then, fatigue accumulation damage is calculated upon every material plane via the fatigue damage accumulation law. Furthermore, by comparing the fatigue damage upon all material planes, the plane with the largest fatigue accumulation damage is determined as the critical plane for the investigated multiaxial loading history, and the ultimate fatigue life of the entire loading history is identified as the fatigue lifetime with regard to this critical plane.

The objective of current work is to put forward a novel calculation method for identifying the direction angle of critical plane under variable amplitude multiaxial loadings. Within the presented method, a critical plane calculation method, which is upon the basis of the largest fatigue damage plane, is presented for multiaxial variable amplitude loading. The presented method can take consideration of the material failure mode. If the material exhibits shear failure mode, the FS damage model is assigned to evaluate fatigue damage for each counted reversal. Otherwise, the SWT damage model is selected to calculate fatigue damage within each counted reversal. The presented critical plane determination approach is deemed to consider the main fatigue damage mechanism during the multiaxial fatigue failure course. Moreover, the proposed critical plane determination framework can be extended to be utilized with stress-based fatigue criteria. Six kinds of materials are selected to verify the accuracy of proposed critical plane determination method. At last, integrating the presented critical plane calculation approach with multiaxial cycle counting approach and fatigue damage accumulation law, a multiaxial fatigue lifetime evaluation technique is presented to predict fatigue lifetime for the investigated seven materials.

2. Calculation of stress and strain parameters on candidate material plane

2.1. Three-dimensional stress state

As depicted within Fig. 1a, the following strain and stress tensors are employed to denote the real elastic–plastic stress and strain states for a generic material point O:

$$\sigma_{ij}=\begin{bmatrix} \sigma_x & \tau_{xy} & \tau_{xz} \\ \tau_{xy} & \sigma_y & \tau_{yz} \\ \tau_{xy} & \tau_{yz} & \sigma_z \end{bmatrix} \tag{4}$$

$$\varepsilon_{ij}=\begin{bmatrix} \varepsilon_x & \varepsilon_{xy} & \varepsilon_{xz} \\ \varepsilon_{xy} & \varepsilon_y & \varepsilon_{yz} \\ \varepsilon_{xz} & \varepsilon_{yz} & \varepsilon_z \end{bmatrix}=\begin{bmatrix} \varepsilon_x & 1/2\gamma_{xy} & 1/2\gamma_{xz} \\ 1/2\gamma_{xy} & \varepsilon_y & 1/2\gamma_{yz} \\ 1/2\gamma_{xz} & 1/2\gamma_{yz} & \varepsilon_z \end{bmatrix} \tag{5}$$

By using the normal vector $\vec{X'}$ of the material plane Δ, the direction of a generic material plane Δ is able to be determined as illustrated in Fig. 1b. The normal vector $\vec{X'}$ is denoted via

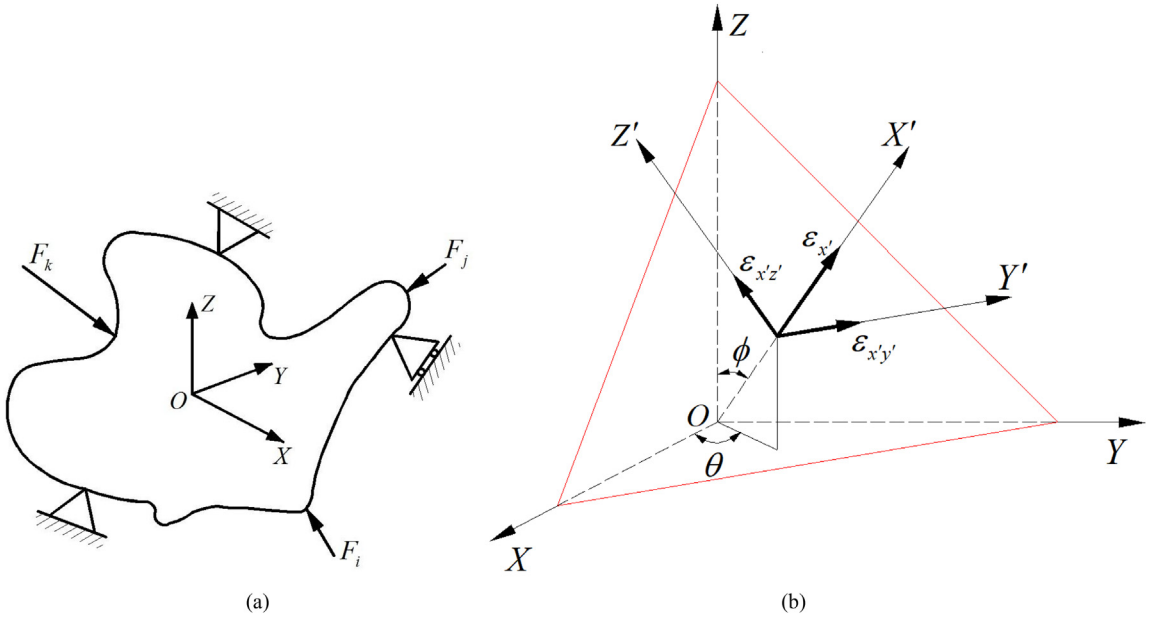

Fig. 1 – Generic material plane Δ and definition of angles ϕ and θ.

orientation angles θ and ϕ. ϕ is the angle between the normal vector $\overrightarrow{X'}$ and Z-axis, and θ is the angle between the projection of normal vector $\overrightarrow{X'}$ upon the X–Y plane and X-axis. Moreover, as shown within Fig. 1b, an innovative reference coordinate system $OX'Y'Z'$ can be obtained, within which Z′-axis is located on the plane Δ, and Y′-axis is located along the intersecting line of generic material plane Δ and the X–Y plane.

The steps for calculating the stress and strain parameters can be summed up as follows.

1. By utilizing angles θ and ϕ, the stress and strain tensors upon the i th candidate material plane Δ can be computed using the following expressions:

$$\sigma'_{ij} = M\sigma_{ij}M^T \tag{6}$$

$$\varepsilon'_{ij} = M\varepsilon_{ij}M^T \tag{7}$$

where M^T is the transpose of transformation matrix M calculated by utilizing the expression as follow:

$$M = \begin{bmatrix} \cos\theta\sin\phi & \sin\theta\sin\phi & \cos\phi \\ -\sin\theta & \cos\theta & 0 \\ -\cos\theta\cos\phi & -\sin\theta\cos\phi & \sin\phi \end{bmatrix} \tag{8}$$

2. Upon the w th candidate material plane, the shear strain range can be calculated by angles θ and ϕ.

$$\Delta\gamma_i = \max_{\substack{t_{start}\le t_1\le t_{end} \\ t_p < t_2 \le t_{end}}} \left\{ 2\sqrt{\left[\varepsilon_{x'y'}(t_1) - \varepsilon_{x'y'}(t_2)\right]^2 + \left[\varepsilon_{x'z'}(t_1) - \varepsilon_{x'z'}(t_2)\right]^2} \right\} \tag{9}$$

where t_{start} and t_{end} are respectively the starting time instant and ending time instant within one reversal. Upon every candidate material plane, the range of shear strain can be determined by making angles θ and ϕ change between 0° and 360° and 0° and 180°. Next, the largest shear strain range and the orientation angle of the largest shear strain range plane are able to be obtained.

3. Upon the i th candidate plane (plane Δ), the normal strain ranges can be computed by utilizing Eq. (10) as follow:

$$\Delta\varepsilon_i = \max_{\substack{t_{start}\le t_1\le t_{end} \\ t_p < t_1 \le t_{end}}} \{|\varepsilon_{x'}(t_1) - \varepsilon_{x'}(t_2)|\} \tag{10}$$

Similarly, by making angles θ and ϕ change between 0° and 360° and 0° and 180°, respectively, the normal strain ranges can be computed upon every candidate material plane. Subsequently, the range of the largest normal strain $\Delta\varepsilon_{max}$ and the orientation angles of the $\Delta\varepsilon_{max}$ planes are able to be obtained via making a comparison of the normal strain range upon every material plane.

4. Upon the i th candidate material plane (plane Δ), the largest normal stress can be calculated by utilizing Eq. (11).

$$\sigma_{n,max} = \max_{t_{start}\le t\le t_{end}} \sigma_{x'}(t) \tag{11}$$

where $\sigma_{x'}(t)$ is the normal stress upon the material plane with regard to all time instants within a counted cycle/reversal.

2.2. Plane stress state

As shown within Fig. 2a, a thin-walled tube component experiences complex tension-torsion loadings, the imposed stresses and strains are expressed as Eqs. (12) and (13):

$$\sigma_{ij} = \begin{bmatrix} \sigma_x & \tau_{xy} & 0 \\ \tau_{xy} & 0 & 0 \\ 0 & 0 & 0 \end{bmatrix} \tag{12}$$

$$\varepsilon_{ij} = \begin{bmatrix} \varepsilon_x & \varepsilon_{xy} & 0 \\ \varepsilon_{xy} & -\nu_{eff}\varepsilon_x & 0 \\ 0 & 0 & -\nu_{eff}\varepsilon_x \end{bmatrix} = \begin{bmatrix} \varepsilon_x & 1/2\gamma_{xy} & 0 \\ 1/2\gamma_{xy} & -\nu_{eff}\varepsilon_x & 0 \\ 0 & 0 & -\nu_{eff}\varepsilon_x \end{bmatrix} \tag{13}$$

where ν_{eff} is the effective Poisson's ratio calculated by using Eq. (14):

$$\nu_{eff} = 0.5 - \frac{(0.5-\nu_e)\Delta\sigma_{eq}}{E\Delta\varepsilon_{eq}} \tag{14}$$

where $\Delta\sigma_{eq}$ and $\Delta\varepsilon_{eq}$ are respectively the von Mises equivalent stress and strain ranges, E is the elastic modulus, and ν_e is the elastic Poisson's ratio. The calculation procedure of effective Poisson's ratio can be found in [29].

Three stresses are equaled to 0 upon the specimen surface for plane stress state, as depicted within Fig. 2b. The material planes in this investigation are all orthogonal to the surface of specimen. Within such a situation, the orientation angle ϕ is equal to 90°, i.e. $\phi = 90°$. Therefore, the investigated material plane Δ is a function of only one orientation angle θ, and θ ranges from 0° to 180°, or from −90° to 90°.

As depicted in Fig. 2b, the θ plane can be denoted as the plane with the normal vector $\overrightarrow{X'}$ at angle θ to X-axis. Upon the θ plane, the shear and normal stresses/strains can be denoted as the following equations:

$$\varepsilon_\theta = \frac{1-\nu_{eff}}{2}\varepsilon_x + \frac{1+\nu_{eff}}{2}\varepsilon_x\cos(2\theta) + \frac{\gamma_{xy}}{2}\sin(2\theta) \tag{15}$$

$$\gamma_\theta = (1+\nu_{eff})\varepsilon_x\sin(2\theta) - \gamma_{xy}\cos(2\theta) \tag{16}$$

$$\sigma_\theta = \frac{1}{2}\sigma_x + \frac{\sigma_x}{2}\cos(2\theta) + \tau_{xy}\sin(2\theta) \tag{17}$$

$$\tau_\theta = \frac{\sigma_x}{2}\sin(2\theta) - \tau_{xy}\cos(2\theta) \tag{18}$$

Subsequently, the stress and strain parameters $\Delta\gamma_{max}$, $\Delta\varepsilon_{max}$ and $\sigma_{n,max}$ on the candidate material planes can be calculated by Steps 2, 3 and 4 in Section 2.1 when the orientation angle ϕ is taken as 90°, namely, $\phi = 90°$.

3. Presented approach for calculating the critical plane

Fatigue crack behavior are systematically investigated under multiaxial load by a lot of researchers, including Carpinteri and co-workers [22] and Fatemi and Shamsaei [28], it can be found that cracks nucleate and propagate upon preferred planes rather than with random orientation. The preferred

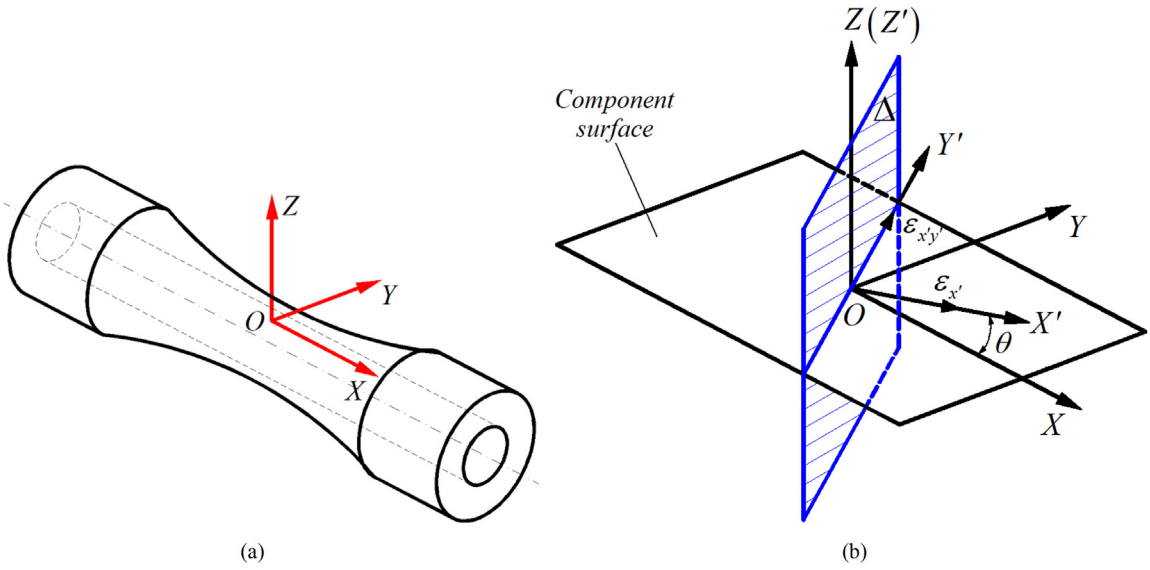

Fig. 2 – (a) Thin-walled tubular specimen subjected to combined tension and torsion loading. (b) Material plane Δ perpendicular to the component surface and having normal vector X′ at angle θ to the X-axis.

orientation relies on the loading state and material type. Moreover, the multiaxial fatigue damage, which is produced via the normal strain/stress and shear strain/stress acting upon the material plane, can contribute to the local plastic deformation. The maximum fatigue damage plane within each counted cycle is constant for constant amplitude multiaxial loading. Whereas, the orientation angles of the maximum fatigue damage planes change within every counted reversal for variable amplitude multiaxial loading, which makes the critical plane determination a tricky problem. In this study, employing an averaging method via an appropriate weight function, which is deemed to consider the primary fatigue damage causes and mechanisms affecting the fatigue failure course to determine a single plane as the critical plane, seems to be reasonable [30,31].

Via averaging the direction angles of largest fatigue damage planes within all counted reversals, the direction angle of the critical plane is able to be calculated for the whole variable amplitude loading history:

$$\overline{\phi} = \frac{1}{\sum_{k=1}^{m} w(k)} \sum_{k=1}^{m} \phi_{cr}(k) w(k) \tag{19}$$

$$\overline{\theta} = \frac{1}{\sum_{k=1}^{m} w(k)} \sum_{k=1}^{m} \theta_{cr}(k) w(k) \tag{20}$$

where $\theta_{cr}(k)$ and $\phi_{cr}(k)$ are used to express the direction angle of the largest fatigue damage plane, m is the total number of reversals, $w(k)$ is the weight function, which can be presented as Eq. (21):

$$w(k) = D_k \tag{21}$$

where D_k is the fatigue damage for k th reversal.

The fatigue damage D_k for k th counted reversal should be calculated in order to determine the weight function in Eq. (21). Systematic research of fatigue crack behavior under multiaxial loadings by a few researchers reveals that investigated materials exhibit two different kinds of failure patterns, namely shear cracking failure pattern and tensile cracking failure pattern, which is dependent upon the physical mechanism of materials and loading conditions [10]. Some materials exhibit tensile cracking behavior where cracks are initiated on the plane experiencing largest normal stress, and some materials display shear cracking behavior where fatigue cracks are observed on the plane of maximum shear amplitude. Other materials exhibit a mixed cracking behavior where cracks are initiated on the largest shear plane for torsional loading but on maximum normal plane for tension–compression loading. In order to account for the different fatigue crack behaviors, suitable fatigue damage criteria should be selected. Experimental data reported in pieces of literature depict at least two kinds of multiaxial fatigue damage criteria are needed: One for tensile cracking failure pattern and another for shear cracking failure pattern.

For materials that show shear fatigue crack failure pattern, Socie and Fatemi [13] presented a multiaxial fatigue damage pattern i.e.

$$\frac{\Delta\gamma_{max}}{2}\left(1 + K\frac{\sigma_{n,max}}{\sigma_y}\right) = \frac{\tau_f'}{G}(2N_{fs})^{b_0} + \gamma_f'(2N_{fs})^{c_0} \tag{22}$$

where σ_y is the yield stress, $\Delta\gamma_{max}/2$ is the amplitude of largest shear strain, $\sigma_{n,max}$ is the largest normal stress, and K is an empirical parameter. It should be pointed out that, for the FS damage model, the plane experiencing the largest amplitude of torsional strain is originally considered as the critical plane, which is always utilized in the analysis of relatively short multiaxial loading sequences composed of repeating cycles. Whereas, the definition of critical plane is slightly modified for multiaxial variable amplitude loading history. Within the present work, the plane with the largest fatigue accumulation damage is defined as the critical plane for material showing

shear cracking failure mode. According to the investigation in [9], the predicted failure plane with the largest fatigue damage is very close to the actual failure plane or the largest shear plane [9].

Within the present study, the similar critical plane definition is utilized for the materials displaying tensile cracking failure mode. For materials showing tensile cracking failure pattern, Socie et al. [32] proposed the critical plane form of SWT parameter [12], which is used for multiaxial proportional and non-proportional fatigue lifetime estimation. The multiaxial fatigue damage model proposed by Socie et al. [32] is shown as follow:

$$\frac{\Delta\varepsilon_{\max}}{2}\sigma_{n,\max}=\frac{\left(\sigma_f'\right)^2}{E}\left(2N_{ft}\right)^{2b}+\sigma_f'\varepsilon_f'\left(2N_{ft}\right)^{b+c} \tag{23}$$

where $\Delta\varepsilon_{\max}/2$ is denoted as the amplitude of normal strain upon the plane experiencing the maximum tensile strain amplitude, and $\sigma_{n,\max}$ is the largest normal stress upon this plane. For materials showing tensile cracking failure pattern, the plane with the largest amplitude of tensile strain is usually considered as critical plane under constant amplitude loading. An alternate definition can be the SWT damage parameter. It should be mentioned that both the definitions can contribute to almost the identical fatigue damage parameter as reported in [10]. Therefore, the critical plane for material showing tensile cracking failure pattern is denoted as the material plane with the largest fatigue damage in the current investigation.

In this study, if the material shows tensile failure mode, the SWT damage model is selected to evaluate fatigue damage D_k for the k th reversal, i.e. $D_k = 1/N_{ft,k}$. On the other hand, if the material exhibiting shear failure mode, the FS damage model is selected to evaluate fatigue damage D_k for the k th reversal, i.e. $D_k = 1/N_{fs,k}$. Hence, the proposed weight function, which can take into consideration of fatigue crack failure modes for different materials, is shown as follow:

$$w(k)=D_k=\begin{cases}\dfrac{1}{2N_{ft,k}} & \textit{for material showing tensile failure mode}\\ \dfrac{1}{2N_{fs,k}} & \textit{for material showing shear failure mode}\end{cases} \tag{24}$$

The proposed weight function expresses the contribution of the direction angle of largest damage plane (denoted by $\phi_{cr}(k)$ and $\theta_{cr}(k)$) to the determination of the critical plane direction angle (denoted by $\overline{\phi}$ and $\overline{\theta}$) for the whole block loading history. It can be found that the larger the fatigue damage D_k is, the more significant the effect of the weight function upon the averaging process becomes.

For material showing shear failure mode, the FS model (Eq. (22)) is used for calculating multiaxial fatigue damage D_k. Therefore, the main fatigue damage driving parameter is regarded as the largest shear strain amplitude ($\Delta\gamma_{\max}^{(k)}/2$) on the largest fatigue damage plane. The secondary prominent damage parameter is considered as the normal stress ($\sigma_{n,\max}^{(k)}$) upon the largest fatigue damage plane. These two damage parameters are both considered in the proposed critical plane determination method. On the other hand, for material showing tensile failure mode, the SWT model (Eq. (23)) is selected to evaluate fatigue damage D_k. Hence, the main fatigue damage driving parameter is regarded as the maximum tensile strain amplitude ($\Delta\varepsilon_{\max}^{(k)}/2$) upon the largest damage plane, and the normal stress ($\sigma_{n,\max}^{(k)}$) acting upon the largest damage plane is considered as the secondary prominent parameter. These two important damage parameters are both considered in the proposed critical plane determination approach. Therefore, the presented critical plane determination method can reflect the main fatigue damage mechanisms for materials showing shear failure mode and tensile failure mode.

For a component experiencing multiaxial variable amplitude loadings, the critical plane is able be obtained by using the presented method, as shown in Fig. 1a. Particularly, if a total number of m loading cycles are counted for the multiaxial constant amplitude loading sequence, the calculated fatigue damage D_k can be identical with $k = 1, 2, \ldots, m$. Hence the computed $w(k)$ value of the proposed weight function (24) is a constant quantity with regard to the counted m loading cycles. This means that the direction angle of critical plane calculated for the whole loading history is in accord with the direction of the critical plane determined within each counted cycle. In such situation, the presented weight function method is unnecessary. In addition, for thin-walled tube component experiencing complex axial-torsional loadings, as seen in Fig. 2a, the candidate material planes are all orthogonal to the surface of investigated component, which means $\phi = 90^\circ$, and the critical plane is able to be calculated using only one angle parameter θ. Within such case, the multiaxial fatigue damage upon the planes of direction angle θ between 0° and 180° is computed by an incremental angle of one degree, and the fatigue damage upon the plane of largest damage can be denoted as D_k within the k th counted reversal.

Subsequently, experimental observations of Inconel 718 reveal that extensive shear cracking exists for both tension and torsion experiments. Thus, the Inconel 718 shows shear failure behavior. On the basis of the presented critical plane determination method, the FS damage parameter (Eq. (22)) is selected to evaluate fatigue damage D_k due to the Inconel 718 displaying shear cracking failure mode. It should be noted that, for pure torsional loading condition, the predicted results are in a difference of $\pm10^\circ$ from the planes of the maximum shear strain amplitude. The 10° deviation from the largest shear plane is due to the normal stress term ($\sigma_{n,\max}$). Consequently, the predicted maximum damage planes are slightly different from the maximum shear planes. However, this problem is not felt to be significant since the predicted failure plane is very adjacent to the largest shear plane or the actual failure plane [9].

Moreover, it should be noted that, some materials fails by the propagation of a mode II shear crack or a mode I tensile crack relying upon the cyclic strain amplitude and stress state [10]. It was reported that, except for the high strain torsion experiments in [10], AISI Type 304 stainless steel tends to produce fatigue crack upon planes of the largest tensile strain. When the tubular specimen made of AISI Type 304 stainless steel is loaded with uniaxial tension-compression loading, the experimentally observed failure plane is orthogonal to the loading direction. That is to say, the AISI Type 304 stainless steel exhibits tensile failure mode in such case. According to

the proposed critical plane calculation approach, the tensile-type fatigue damage model, SWT model (Eq. (23)) is selected to evaluate fatigue damage D_k. It should be pointed out that the maximum fatigue damage plane estimated via the presented method is located at the material plane with $\theta_{cr}(k) = 0°$. In other words, the direction angle of critical plane predicted by the presented method can be oriented at $\overline{\theta} = 0°$. The prediction result is consistent with the experimental observation as shown in [10]. On the other hand, when the tubular specimen made of AISI Type 304 stainless steel is subjected to pure torsional loading, shear nucleation can be found within the tested AISI Type 304 stainless steel [10]. It implies the AISI Type 304 stainless steel shows shear cracking failure mode in such instance. Based on the proposed critical plane calculation method, the shear-type fatigue damage model, FS model (Eq. (22)) is selected to evaluate fatigue damage D_k. Experimental observations reveal that the predicted critical plane with largest fatigue damage can correlate well with the actual failure plane [9].

In addition, if appropriate multiaxial high cycle fatigue criteria are employed, the proposed weight-averaged critical plane can be extended to be utilized with stress-based fatigue criteria. The utilization of proposed critical plane method with stress-based fatigue criteria will be shown within the discussion part.

4. Experimental verification

Five types of materials, namely, titanium alloy BT9 [23], pure titanium [23], 304L stainless steel [24], 1050 QT steel [24] and sintered iron [33] are selected to validate the validity of proposed critical plane determination method. It should be noted that titanium alloy BT9, pure titanium, 304L stainless steel and 1050 QT steel show shear failure mode, and sintered iron exhibits tensile failure mode. For titanium alloy BT9, pure titanium, 304L stainless steel, 1050 QT steel, a closed-loop servo-controlled hydraulic tension-torsion loading frame in conjunction with a digital servo-controller is utilized for performing the experiments. The capacity of the loading cell is 100 kN in axial and 1 kN m in torsion direction. A strain-controlled mode is employed utilizing the extensometer for nearly half the fatigue lifetime. The adoptive frequencies ranged from 0.1 Hz to 3 Hz for purpose of acquiring a near-constant plastic strain rate. Moreover, all multiaxial constant-amplitude fatigue experiments are conducted using ASTM Standard E2207. For sintered iron, the strain-controlled multiaxial fatigue tests are performed in MTS-809 axial/torsional servo-hydraulic testing system at room temperature. The multiaxial testing equipment possesses capability of 2000 Nm in torque and 250 kN in axial load. In the gage section of the thin-walled tube specimen, a MTS axial/torsional extensometer with 25 mm gage length is utilized for measuring the shear and axial strains. The conducted testing frequencies are 0.5 Hz and 0.1 Hz for proportional and non-proportional multiaxial loading paths, respectively. More detailed information of the fatigue tests, geometrical dimensions of the specimens, mechanical parameters, measured orientation angle of the critical plane, chemical compositions of the investigated five materials can be found in [23,24,33].

For titanium alloy BT9 and pure titanium, the selected variable amplitude loading sequences are shown in [23]. Each loading sequence consists of different combinations of three fully-reversed sinusoidal loading types, namely, axial tension-compression, pure torsional, and multiaxial 90° non-proportional loading, as depicted within Fig. 3a–c. Loading sequences A′ and T are composed of one loading type from the fully-reversed pure torsional and axial tension-compression loading. Loading sequences B contains two loading type from the fully-reversed pure torsional, axial tension-compression, and multiaxial 90° out of phase loading, and the second loading type is loaded continually until to fatigue failure. Loading sequences C includes some loading blocks, which are made up from the above-mentioned three loading paths, and each loading block is repeatedly loaded until to finial fatigue failure. Moreover, two complex loading block sequences CL1 and CL2, which are composed of frequent variation of above-mentioned three loading paths, are performed on thin-walled tubular specimens of titanium alloy BT9. It should be noted that loading block sequences B, C, CL1 and CL2 are conducted under the identical equivalent strain amplitude.

Then, for 1050 QT steel and 304L stainless steel, four tension-torsion loading histories, i.e. FRI, FRI15, FRR, and PI from [24] are also employed in the current investigation. FRR and FRI paths are composed of 360 in-phase fully-reversed cycles. FRI loading path starts from the axial tension-compression cycle with 1° increment, as shown within Fig. 3d, and FRR strain path is applied within a random manner, as shown in Fig. 3e. Compared with FRI path, FRI15 path also starts from the axial tension-compression cycle, however, the angle increment of FRI15 strain path is 15° instead of 1°, as illustrated in Fig. 3f. PI path begins from the pure axial cycle with 1° increment, and includes 360 in-phase pulsating axial-torsional cycles, as depicted in Fig. 3g. FRI90 path contains two kinds of loading cycles, namely, tension-compression and torsional loading cycles. Moreover, FRI90 path begins from axial tension-compression cycle, and each loading block including four fully-reversed cycles, as show in Fig. 3h. Subsequently, compared with FRI90 path, PI90 path is pulsating as depicted in Fig. 3i.

Subsequently, for sintered iron, seven kinds of multiaxial in-phase and out-phase strain paths have been selected in order to validate the presented critical plane determination method, that are A, B, D, G, H, I and J paths from [33] as shown in Fig. 3. Path G denote compression and torsion loading path with $\Delta\varepsilon/\Delta\gamma = -0.3$, Path H is elliptical shape load path with 90° phase angle, Path I and J express double and triangular strain paths, respectively.

Based on the proposed critical plane determination approach, the orientation angles of critical plane can be predicted for the investigated several loading paths. Comparison of the estimated orientation angles of critical planes and the experimental measures are depicted within Fig. 4a–e. It should be mentioned that, the presented method can well estimate the orientation angle of critical plane, the deviations are basically 10° between the prediction results and the experimentally measured crack directions with regard to the selected five materials. Moreover, the prediction performances of other models are shown in [23,24,33]. It can be found that, the proposed approach can give more satisfactory

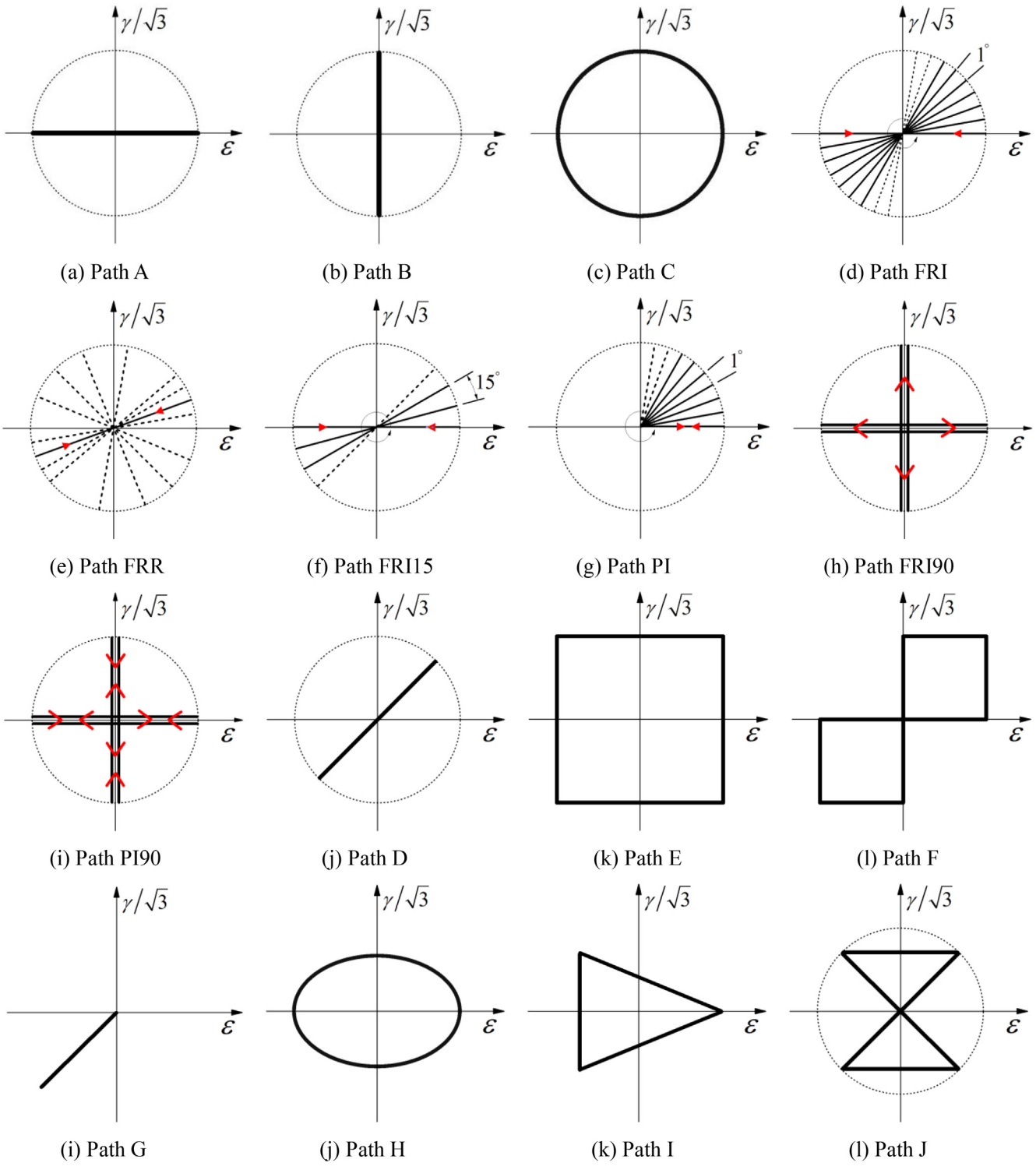

Fig. 3 – Loading paths utilized in this investigation [10,23,24,33].

estimation results. According to the critical plane analysis within this section, the proposed method shows a good estimation of critical plane orientation angles with regard to the investigated five kinds of materials. Therefore, the presented approach is able to be utilized to evaluate critical plane direction for multiaxial variable amplitude loadings.

5. Multiaxial fatigue lifetime estimations according to presented critical plane determination method

Multiaxial fatigue lifetime can be estimated according to the presented weight-averaged critical plane calculation method.

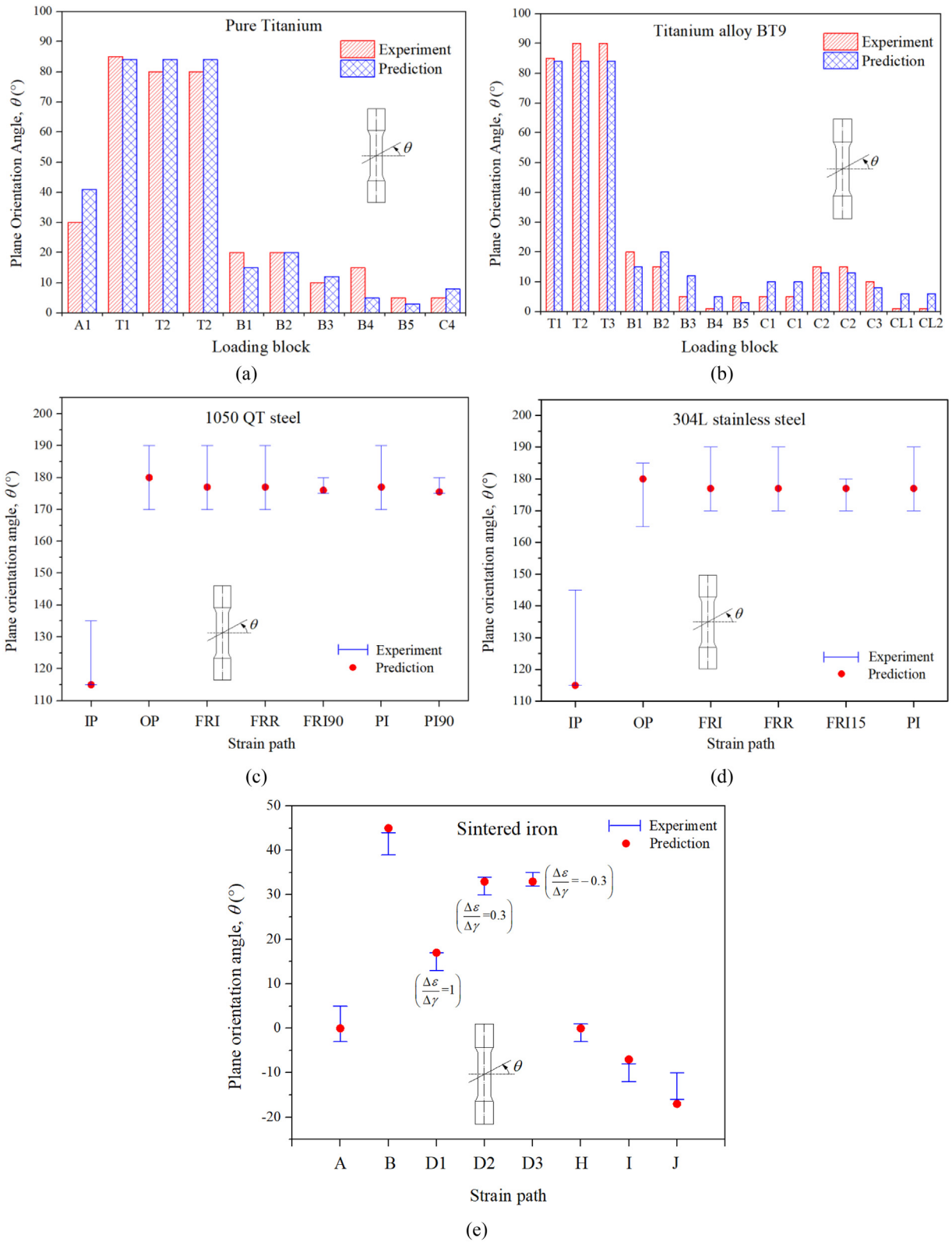

Fig. 4 – Comparisons of critical plane orientation predicted by the proposed approach and experimentally observed failure plane orientation under variable amplitude block loading for (a) pure titanium, (b) titanium alloy BT9, (c) 1050 QT steel, (d) 304L stainless steel and (e) sintered iron.

As depicted in Fig. 5, the flow diagram of presented fatigue lifetime evaluation is shown under multiaxial variable amplitude loadings.

5.1. *Multiaxial cycle count*

A suitable cycle count approach is required in order to extract some isolated cycles for multiaxial variable amplitude loading history. Based on the simple uniaxial rainflow counting technique, Langlais et al. [34] proposed a multiaxial cycle count approach, in which multiaxial load sequence can be categorized into two channels, namely, master and auxiliary counting channels. For the main counting channel, this counting method can be used to count cycles. Meanwhile, some crucial contents in the auxiliary counting channels can be saved. For variable amplitude multiaxial loading, the multiaxial cycle count approach given by Langlais et al. [34] is widely performed to extract cycles.

The important processes in the Langlais et al.'s multiaxial cycle count approach are able to be shown in the following steps.

1. A data stack can be established, which relies merely upon the number of selected counting channels. Each line of the statistical stack includes the values of all counting channels at a given sample or time. Moreover, when one channel is defined as the master counting channel in the statistical stack, the others are selected as auxiliary counting channels. Next, fatigue test data are successively read and put into the statistical stack.
2. The test data can be discarded from the statistical stack when a fatigue test data point cannot construct a reversal within the master counting channel, simultaneously, the critical content for discarded test data can be conserved in the auxiliary counting channels.
3. The symbol X is used to denote the strain range within the current time, which is constructed using the uppermost two data points in the statistical stack. In addition, the symbol Y is used to represent the prior strain range which is located adjacent to the range X. If strain range X is larger than Y, i.e. $X \geq Y$, Y is considered as a completed cycle.

In order to explain the concept of Langlais's multiaxial counting approach clearly, a tension-torsion variable amplitude loading sequence is employed as shown in Fig. 6. For this selected multiaxial loading history, two cycles are counted according to Langlais's counting approach, containing a larger cycle constructed by 0-3-4 with shear strain range $\Delta\gamma = 3500\mu\varepsilon$ and a smaller cycle constructed by 1-2-3 with shear strain range $\Delta\gamma = 1500\mu\varepsilon$.

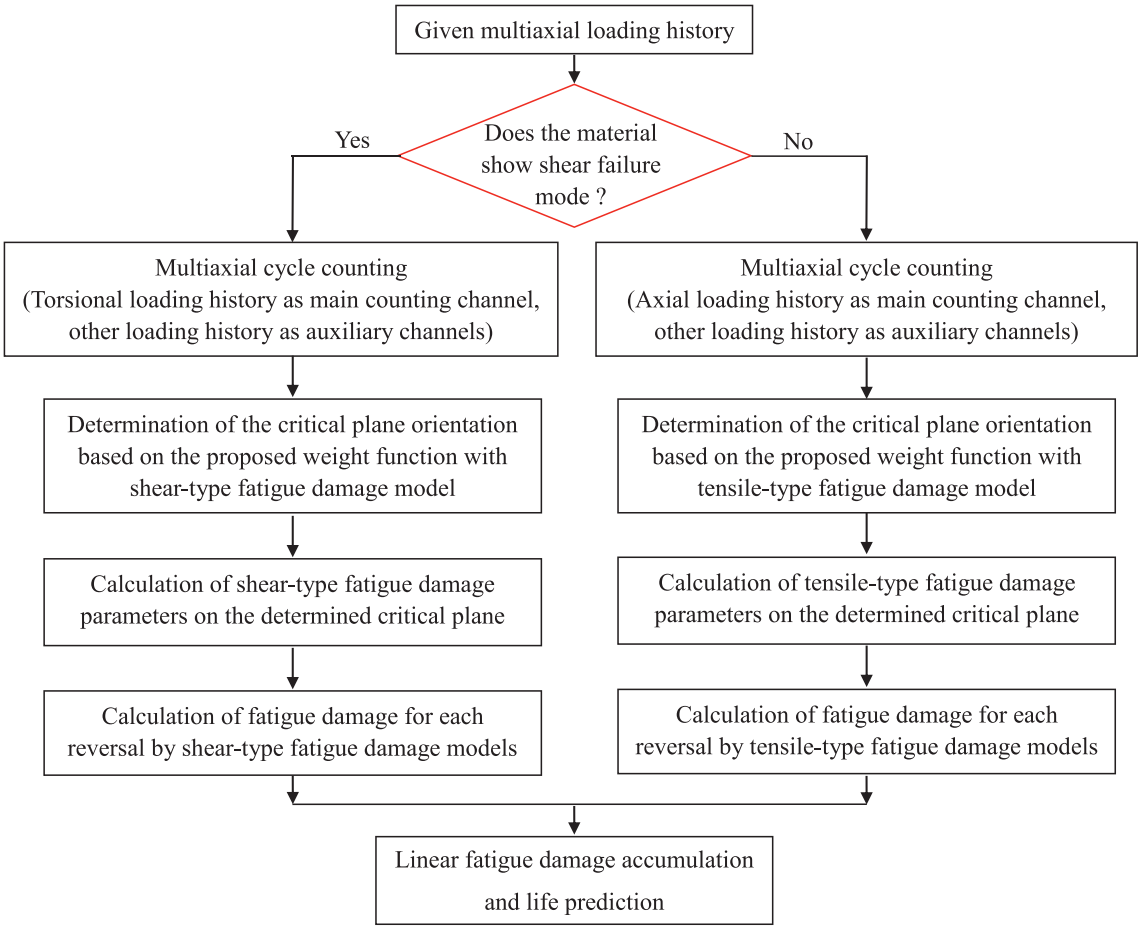

Fig. 5 – Flow chart of proposed fatigue life prediction under variable amplitude multiaxial loading.

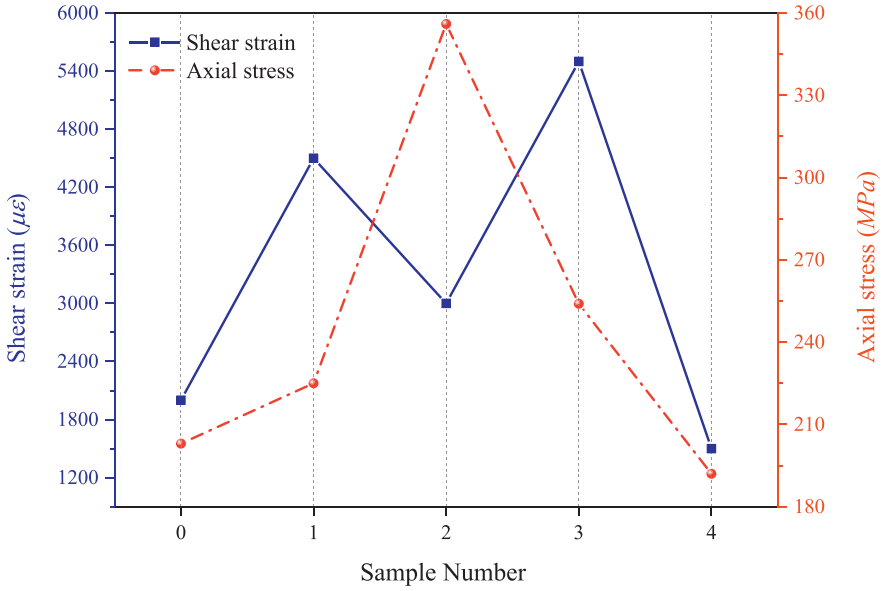

Fig. 6 – Strain–number variable amplitude axial and torsional loading histories.

5.2. *Computation of multiaxial fatigue damage quantities upon weight-averaged critical plane*

The orientation angles of critical plane, which is denoted by angles $\overline{\phi}$ and $\overline{\theta}$ can be obtained according to the proposed weight-averaged critical plane determination approach. Then, by employing Eqs. (25) and (26), the stress and strain tensors can be computed on the critical plane:

$$\sigma'_{ij} = M_{cr}\sigma_{ij}{M_{cr}}^{T} \tag{25}$$

$$\varepsilon'_{ij} = M_{cr}\varepsilon_{ij}{M_{cr}}^{T} \tag{26}$$

where the transformation matrix M_{cr} can be computed by Eq. (27):

$$M_{cr} = \begin{bmatrix} \cos\overline{\theta}\sin\overline{\phi} & \sin\overline{\theta}\sin\overline{\phi} & \cos\overline{\phi} \\ -\sin\overline{\theta} & \cos\overline{\theta} & 0 \\ -\cos\overline{\theta}\cos\overline{\phi} & -\sin\overline{\theta}\cos\overline{\phi} & \sin\overline{\phi} \end{bmatrix} \tag{27}$$

Subsequently, a specific presentation of the calculation of multiaxial fatigue damage quantities is able to be provided as follows.

1. Upon the weight-averaged critical plane, the largest shear strain range ($\Delta\gamma^{cr}_{max}$) is able to be determined by Eq. (28):

$$\Delta\gamma^{cr}_{max} = \max_{\substack{t_{start}\le t_p\le t_{end}\\ t_1<t_q\le t_{end}}} \left\{ 2\sqrt{\left[\varepsilon_{x'y'}(t_p)-\varepsilon_{x'y'}(t_q)\right]^2+\left[\varepsilon_{x'z'}(t_p)-\varepsilon_{x'z'}(t_q)\right]^2} \right\} \tag{28}$$

where t_p and t_q are utilized to express a couple of time points when the largest shear strain amplitude is achieved in a counted reversal.

2. Upon the weight-averaged critical plane, the largest normal stress $\sigma^{cr}_{n,max}$ is able to be computed utilizing Eq. (29).

$$\sigma^{cr}_{n,max} = \max_{t_{start}\le t\le t_{end}} \sigma_{x'}(t) \tag{29}$$

where $\sigma_{x'}(t)$ is the normal stress with regard to all time instants within a counted reversal upon the critical plane.

3. Upon the weight-averaged critical plane, the largest normal strain range $\Delta\varepsilon^{cr}_{max}$ can be computed by using the expression as follow:

$$\Delta\varepsilon^{cr}_{max} = \max_{\substack{t_{start}\le t_m\le t_{end}\\ t_p<t_n\le t_{end}}} \{|\varepsilon_{x'}(t_m)-\varepsilon_{x'}(t_n)|\} \tag{30}$$

where t_m and t_n are utilized to express a couple of time points when the largest normal strain amplitude is achieved in a counted reversal.

5.3. *Multiaxial fatigue accumulation damage*

When the fatigue damage is computed with respect to every counted reversal, accumulated fatigue damage D for whole load history is able to be computed by employing the linear damage accumulation law presented by Miner:

$$D = \sum_{k=1}^{m} \frac{1}{2N_{f,k}} \tag{31}$$

where $N_{f,k}$ is the fatigue life with regard to the k th counted reversal, m is the total number of reversals.

At last, the estimated fatigue lifetimes is able to be calculated using the formula as follow:

$$N_{pre} = \frac{1}{D} \tag{32}$$

Table 1 – Fatigue properties of the investigated materials.

Material	Ref.	E (GPa)	G (GPa)	ν_e	σ'_f (MPa)	ε'_f	b	c	τ'_f (MPa)	γ'_f	b_0	c_0	K
Pure titanium	[23]	112	40	0.4	647	0.548	−0.033	−0.646	485	0.417	−0.069	−0.523	0.6
Titanium alloy BT9	[23]	118	43	0.37	1180	0.278	−0.025	−0.665	881	0.18	−0.082	−0.47	0.5
1050 QT steel	[24]	203	81	0.27	1346	2.01	−0.062	−0.725	777	3.481	−0.062	−0.725	0.6
304L stainless steel	[24]	195	77	0.27	1287	0.122	−0.145	−0.394	743	0.2113	−0.145	−0.394	0.15
AISI Type 304 stainless steel	[10]	183	82.8	0.3	1000	0.171	−0.114	−0.402	709	0.413	−0.121	−0.353	–
Sintered iron	[33]	162	–	–	289	0.047	−0.074	−0.406	–	–	–	–	–

5.4. *Multiaxial fatigue lifetime estimation results*

In the present study, six sorts of materials containing titanium BT9 [23], pure titanium [23], 304L stainless steel [24], 1050 QT steel [24], AISI Type 304 stainless steel [10] and sintered iron [33] are selected to evaluate the proposed multiaxial fatigue lifetime prediction methodology. It should be pointed out that AISI Type 304 stainless steel and sintered iron exhibits tensile failure mode, and the other four materials show shear failure mode. All of the investigated specimen geometries are thin-walled tube specimens. For the investigated six materials, the mechanical and fatigue properties can be depicted within Table 1, the employed loading paths are depicted within Fig. 3.

As depicted within Fig. 7, estimated fatigue lives are compared with experimental measures for the investigated six kinds of materials under variable amplitude multiaxial loadings. Satisfactory fatigue lifetime predictions are able to be observed using the presented multiaxial fatigue lifetime estimation method, the predicted fatigue lives can be mainly within an error factor of 3. Combined with Figs. 4 and 7, it should be mentioned that orientation angles of fatigue crack initiation planes predicted using the presented critical plane method correlate well with the experimentally observed results. In addition, for various multiaxial loadings as shown in Fig. 7, the predicted fatigue lives of the selected several materials fall basically in an error factor of three according to the presented critical plane approach. Hence, these results certify that the presented approach is capable to estimate the direction angle of fatigue crack initiation plane accurately and supply satisfactory fatigue life assessments for the investigated materials.

It can be concluded that, for the investigated six kinds of materials, the multiaxial fatigue lifetime evaluation technique on account of the presented weight-averaging critical plane approach can supply satisfactory fatigue lifetime estimations. The proposed multiaxial fatigue lifetime estimation methodology is able to be a reasonable and effective technique for the fatigue lifetime estimation of machine parts under multiaxial variable amplitude loading paths.

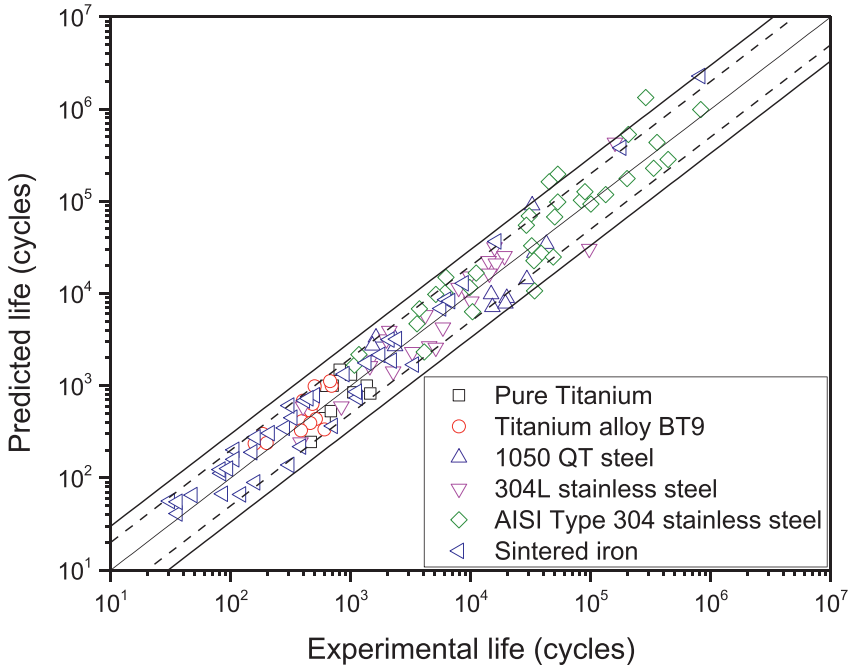

Fig. 7 – Comparison of experimental and predicted fatigue lives based on proposed critical plane approach under variable amplitude block loading for pure titanium, titanium alloy BT9, 1050 QT steel, 304L stainless steel, AISI Type 304 stainless steel and sintered iron.

6. Discussion

Within the critical plane determination method presented by Wang and Wang (Wang and Wang; 2005), the fatigue damage D_i is evaluated using the largest shear strain $\gamma_{max}(t_i)$ at each time point t_i. However, according to the investigation of cracking behaviors for materials exhibiting shear fracture, the maximum shear strain range upon the material plane is able to promote fatigue crack initiation, and the normal stress upon the crack plane can assist in fatigue crack growth. Therefore, for the purpose of predicting fatigue damage accurately, it is universally accepted to select the multiaxial fatigue damage models with the largest shear strain range $\Delta\gamma_{max}$ rather than the largest shear strain γ_{max} [23,24,28]. Hence, the FS damage parameter, which contains the largest shear strain range $\Delta\gamma_{max}$ and normal stress items are able to be utilized to compute the critical plane. When searching for critical plane under variable amplitude multiaxial loadings, those planes experiencing the largest FS damage parameter in each counted reversal can be taken into consideration. Similarly, for materials exhibiting tensile fracture, the plane experiencing the largest SWT damage parameter in all counted reversals can be considered when searching for critical plane under multiaxial variable amplitude loadings. Within this study, for the whole loading sequence, it can be reasonable to calculate the critical plane via averaging the direction angles of material planes with the largest fatigue damage parameters in all counted reversals by an appropriate weight function. Additionally, the predicted results by Wang and Wang and Carpinteri et al. using their proposed weight functions can be seen in [25,26]. In comparison, the proposed approach based on weight-averaged largest fatigue damage critical plane can provide more satisfactory fatigue life predictions in the current study.

It is worth emphasizing that, the process of determining critical plane, which is presented by Shamsaei et al. in [23,24], is time consuming. The orientation angle θ of material planes vary from 0° to 180°, and the cumulative fatigue damage on all investigated material planes need to be computed. Particularly, when nonlinear fatigue damage accumulation laws are employed, fatigue damage on each candidate material plane needs to be accumulated for all counted reversals. In comparison with critical plane method proposed by Shamsaei et al. [23,34], the presented critical plane determination method with this work is able to estimate the orientation angle of fatigue failure plane conveniently. For the investigated titanium alloy BT9, pure titanium, 304L stainless steel, 1050 QT steel and sintered iron, orientation angles of critical plane predicted using the presented method are mainly in the difference of 10° from the measured failure plane orientations. The predictive fatigue lifetimes by Shamsaei et al. are able to be seen within [23,24]. It can be found that the overall predicted results in this work are analogous to those shown by Shamsaei et al. [23,24]. Meanwhile, the multiaxial fatigue life estimations based upon the presented weight-averaged critical plane can supply good prediction abilities in an error factor of 3 (see Fig. 7).

In the current work, the presented weight function can be shown in Eq. (24). With the combination of Eq. (24) and FS and SWT fatigue damage models, it should be mentioned that the multiaxial fatigue damage parameters $\frac{\Delta\gamma_{max}}{2}\left(1+K\frac{\sigma_{n,max}}{\sigma_y}\right)$ and $\frac{\Delta\varepsilon_{max}}{2}\sigma_{n,max}$ are proportional to the proposed weight function $w(k)$, respectively, i.e.

$$\left|\frac{\Delta\gamma_{max}}{2}\left(1+K\frac{\sigma_{n,max}}{\sigma_y}\right)\right| \propto w(k) \tag{33}$$

$$\left|\frac{\Delta\varepsilon_{max}}{2}\sigma_{n,max}\right| \propto w(k) \tag{34}$$

For material showing tensile failure mode or shear failure mode, appropriate multiaxial fatigue damage models are selected to estimate fatigue damage within the proposed weight-averaged critical plane determination approach. It should be mentioned that the larger the multiaxial fatigue damage parameter is, the more prominent the effect of proposed weight function upon the average process makes. Therefore, the proposed approach reflects the dominating fatigue damage mechanisms for materials showing shear or tensile failure mode. In addition, for out-of-phase or in-phase constant amplitude multiaxial loadings, the proposed weight function $w(k)$ (Eq. (24)) achieves a constant value with regard to all counted reversals. In such situation, the presented weight function method is not needed. In the present study, six sorts of materials including tensile and shear failure materials are employed for estimating the proposed multiaxial fatigue lifetime estimation method. It can be found that most fatigue life prediction results are in an error of 3.

In addition, if a suitable stress-based fatigue criteria is adopted, the presented framework of weight function $w(k)$ method (Eq. (24)) can be extended to be utilized with stress-based fatigue criteria. On account of the critical plane method, Zhang et al. presented a revised stress-based fatigue criterion [35]. The equivalent shear stress amplitude $\tau_{eq,a}$ presented by Zhang et al. [35] is expressed by the following formula:

$$\tau_{eq,a}=\sqrt{C_a^2(\overline{\phi},\overline{\theta})+\left[4\left(\frac{t_{-1}}{f_{-1}}\right)^2-1\right]N_a^2(\overline{\phi},\overline{\theta})+4t_{-1}^2\left(\frac{1}{\sigma_u^2}+\frac{2}{f_{-1}\sigma_u}\right)\cdot Sign(N_m)\cdot N_m^2(\overline{\phi},\overline{\theta})}=C_r\left(N_f\right)^{m_r} \tag{35}$$

where C_r and m_r are the material quantities calculated utilizing torsional S–N curve, respectively, $N_a(\overline{\phi},\overline{\theta})$ is the normal stress range, $C_a(\overline{\phi},\overline{\theta})$ is the shear stress range, $N_m(\overline{\phi},\overline{\theta})$ is the normal

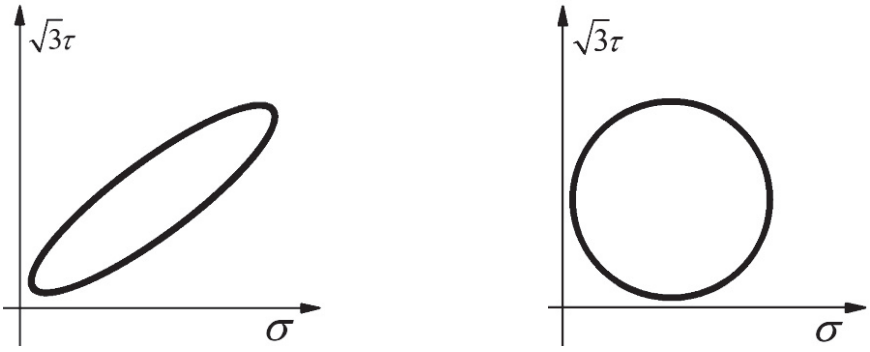

(a) 30° non-proportional loading path (b) 90° non-proportional loading path

Fig. 8 – Multiaxial constant amplitude loading paths for 7050-T651 aluminum alloy thin-walled tubular specimens [36].

mean stress, σ_u is ultimate tensile strength for material, t_{-1} is fully reversed torsional fatigue limit, f_{-1} is fully reversed bending fatigue limit, $Sign(N_m)$ is sign function, which can be expressed as follows:

$$Sign(N_m) = \begin{cases} 1 \ if \quad N_m > 0 \\ -1 \ if \quad N_m < 0 \end{cases} \tag{36}$$

The experimental information of thin-walled tube components made of 7050-T651 aluminum alloy is employed to verify the validity of the presented critical plane calculation method. For 7050-T651 aluminum alloy thin-walled tubular specimens, the details of the mechanical properties, fatigue experiments, specimen geometries, and chemical compositions can be acquired in [36]. Four categories of multiaxial loading sequences are used to verify the presented methodology, which are composed of fully-reversed sinusoidal 30° non-proportional stress path, 90° non-proportional stress path, and two different kinds of multiaxial variable amplitude stress paths (as depicted in Fig. 8, Fig. 9a and b). Furthermore, as shown within Table 2, for the investigated four sorts of multiaxial loading sequences, the predictive direction angle of the critical plane using the presented method are in comparison with the direction angle of experimentally measured failure plane. It can be found that the presented method nicely recognizes the critical plane mostly in the difference of 10° from the experimentally measured crack direction. By means of the critical plane analysis within the stress-based fatigue criteria, the critical plane determined using the presented method shows a good prediction of failure plane direction for the selected materials, particularly within the condition of multiaxial variable amplitude loadings.

Furthermore, multiaxial fatigue lifetime is estimated on the basis of the presented weight-averaged critical plane with stress-based fatigue criteria. Within the current study, experimental data of 2024-T4 and 7075-T651 aluminum alloy smooth thin-walled specimens are used for validating the proposed fatigue lifetime evaluation method. The test data are obtained from [36,37]. The fatigue characters of the selected two materials are shown within Table 3. Moreover, as depicted in Table 4, the S–N cures of 7050-T7451 and 2020-T4 aluminum alloy are shown for fully reversed axial and torsional loadings. For thin-walled specimens made of 7050-T651 aluminum alloy, the variable amplitude multiaxial loading histories utilized within this investigation are depicted in Fig. 9. The fatigue test procedures for thin-walled specimens made of 2024-T4 aluminum alloy are described within [36] in detail. Fatigue test results are depicted within Table 5 under variable amplitude multiaxial loadings. A few constant amplitude loading spectrums are included in the variable amplitude block loadings. Composition and test results of constant amplitude multiaxial load spectrum are shown in Table 6. Subsequently, comparisons of estimated lifetimes based on the presented approach with test data for thin-walled specimens made of 7050-T7451 and 2020-T4 aluminum alloy are shown under variable amplitude block loadings, as depicted within Fig. 10. It can be seen that estimated fatigue lifetimes correlate well with the test results, in which estimated lifetime are basically in an error factor of 3.

With the incorporation of Table 2 and Fig. 10, it can be seen that direction angles of critical planes determined using the presented method correlate well with the experimentally measured failure planes for thin-walled specimens made of 7050-T7451 and 2020-T4 aluminum alloy. In addition, with regard to the investigated multiaxial loading blocks, the predictive fatigue lifetimes upon the basis of the presented critical plane approach are basically within an error factor of three. Hence, the multiaxial fatigue life predictions show that the presented method is able to evaluate the failure planes effectively and supply satisfying lifetime estimations for the selected two materials.

In this study, for the investigated materials exhibiting shear failure or tensile failure, the presented multiaxial fatigue lifetime prediction methodology upon the basis of weight-averaged largest damage plane can be used as an effective fatigue lifetime estimation technique. It can be an accuracy and reliable methodology for the fatigue life

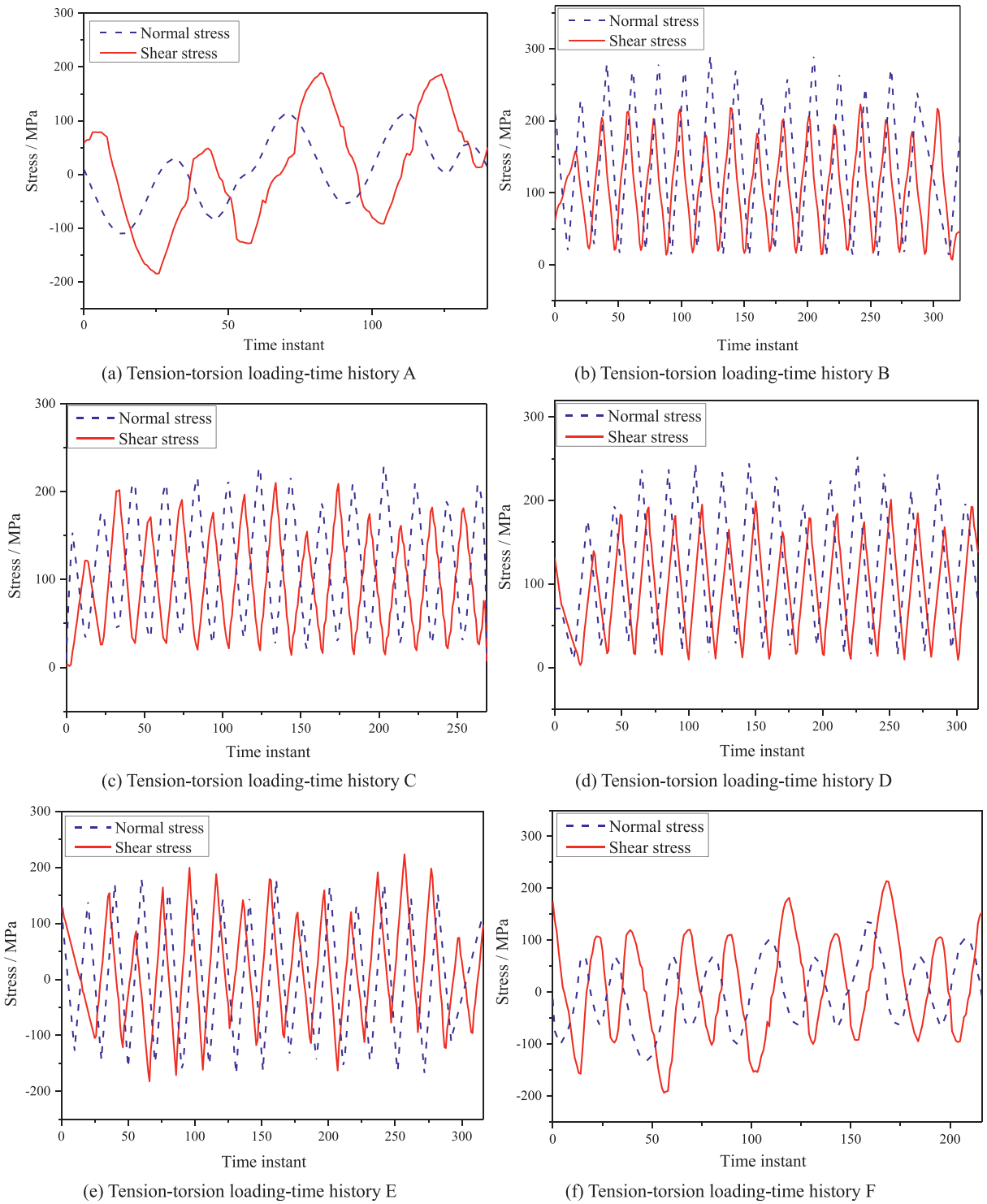

Fig. 9 – Multiaxial variable amplitude loading paths utilized in this investigation [36].

Table 2 – Comparisons between the experimental and the predicted crack initiation plane orientations for 7075-T651 aluminum alloy.

Experimental loading condition	Orientation angle of experimentally observed fatigue crack initiation/ (°)	Orientation angle of predicted fatigue crack initiation/ (°)
30° non-proportional loading path	60	68
90° non-proportional loading path	65	74
Random loading path 1	72	81
Random loading path 2	70	77

Table 3 – Mechanical properties of 7050-T651 and 2024-T4 aluminium alloy [36,37].

Material	E/GPa	ν	G/GPa	σ_y/MPa	σ_u/MPa
7075-T651 aluminium alloy	71.7	0.306	27.5	501	561
2024-T4 aluminium alloy	73	0.33	27.4	400	545

Table 4 – S–N cures of 7050-T651 and 2024-T4 aluminium alloy [36,37].

Experimental loading condition	Fully reversed S–N curve for 7050-T651 aluminium alloy	Fully reversed S–N curve for 2024-T4 aluminium alloy
Axial	$\sigma_{max} = 888.90(N_f)^{-0.10042}$	$\sigma_a = 1207.5(2N_f)^{-0.13564}$
Torsional	$\tau_{max} = 688.85(N_f)^{-0.12233}$	$\tau_{max} = 602.8(2N_f)^{-0.11147}$

Table 5 – Multiaxial fatigue test results for 2024-T4 aluminum alloy under variable amplitude block loadings [37].

Specimen number	Loading spectrum composition	Experimental results (*k*-*X*-*n*)	
201	A-D	17-A-1555	11-A-2204
202	D-A	14-D-1154	13-A-409
203	O–I	8-I-357	8-O-221
401	D-O-I-A	3-I-1036	4-I-1429
402	O-A-D-I	2-O-126	3-O-80
403	I-A-D-O	4-I-2409	4-I-2697
404	D-O-A-I	5-I-320	5-O-136
801	A-P-H-E-M-K-O-I	3-E–352	4-O-50
802	D-L-J-G-B-N-F-H	2-B-117	2-N-69
R01	O-D-G-M-H-F-G-H-O-H-M-J-M-N-J-E-K-F-G-G-K-A-F-N-B-B-B-B-B-I-F-J-P-O-A-B-B-B-B-B-B–B–B–B–B–N–O–B–B–B	26th-B-113	31st-J-57
R02	L-C-A-C-I-G-C-D-B-N-D-P-B-B-G-O-L-I-P-B-D-C-M-P-D-K-L-I-A-L-C-H-M-P-D-A-H-C-I-J-K–H-D-E-F-D-L-O-G-I	25th-K-349	22nd-M-437
R03	O-M-B-B-B-B-B-F-G-E-L-A-M-I-I-B-B-B-B-B-I–H-A-P-H-G-P-I-B-B-B-B-B-J-D-O-P-P-H-O-M-A-H-G-D-K-J-O-L-A	28th-B-182	38th-H-669
R04	E-B-B-B-B-B-E-P-B-B-B-B-B-G-D-K-N-N-F-L-O-G-M-A-P-O-L-E-F-G-I-D-B-B-B-B-B-H-L-J-O–H-M-O-P-D-I-B-B-B	46th-I-620	44th-P-92

Table 6 – Experimental fatigue lives under multiaxial constant amplitude loading for 2024-T4 aluminum alloy [37].

Loading path	σ_a/MPa	σ_m/MPa	τ_a/MPa	τ_m/MPa	δ/°	Fatigue life/cycle
A	250	0	0	0	0	56 316
B	350	0	0	0	0	6167
C	0	0	144.3	0	0	63 795
D	0	0	167	0	0	49 912
E	158.1	0	111.8	0	0	76 451
F	177	0	102.2	0	0	80 107
G	248	0	143	0	0	6488
H	158	0	120	0	30	63 584
I	158	0	125	0	45	57 004
J	248	0	143.2	0	45	7363
K	158	0	132	0	60	30 893
L	177	0	102.2	0	90	49 292
M	158.1	0	139.1	0	90	15 459
N	244	0	157.2	0	90	3453
O	250	0	144.3	0	90	4634
P	250	0	125	0	90	6811

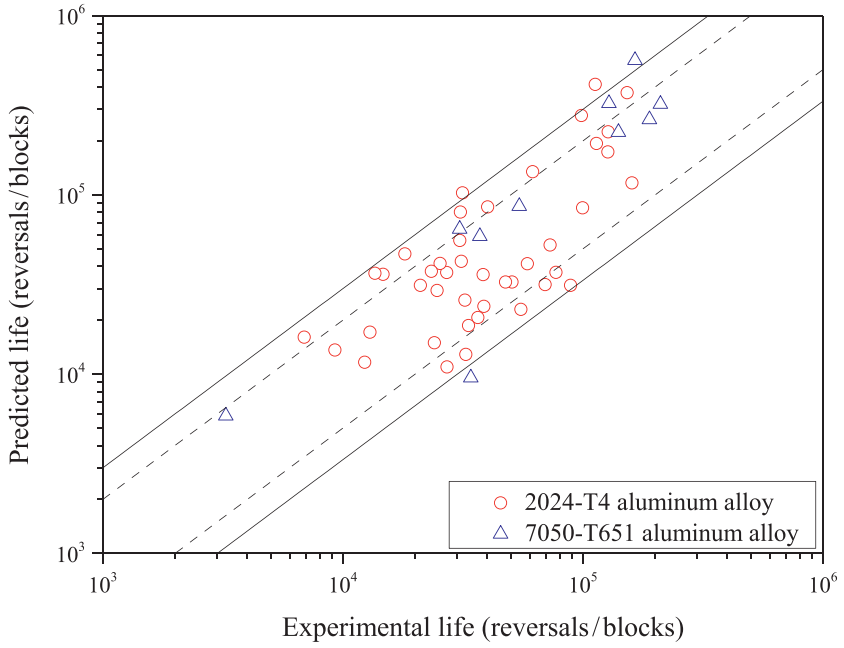

Fig. 10 – Comparison of experimental and predicted fatigue lives based on proposed fatigue life prediction method under variable amplitude block loading.

prediction of machine parts experiencing multiaxial variable amplitude loadings [38–41]. The reliability of the proposed methodology in handling the fatigue lifetime estimation of actual engineering parts [42–46], which are subjected to complicated three-dimension stress states, needs more research [47–52] in the further.

7. Conclusions

A new critical plane determination method is proposed under multiaxial variable amplitude loadings, which is denoted as weight-averaged largest fatigue damage plane. The material failure manners can be considered by the defined weight function, and the proposed critical plane can be utilized with both strain-based and stress-based critical plane models. Based on the proposed critical plane, a multiaxial fatigue lifetime estimation methodology is established for evaluating fatigue life under variable amplitude loading. A total number of eight materials are selected to verify the proposed methodology, the following conclusions can be drawn.

(1) The orientation angles of the failure planes estimated by the presented method can correlate well with experimentally observed failure planes basically in the 10° difference for both shear and tensile failure materials.
(2) On account of the presented critical plane determination method, a specific technique of multiaxial fatigue lifetime evaluation with strain-based critical plane models is proposed in the current study, which can predict fatigue lifetimes satisfactorily under multiaxial variable amplitude loadings, the estimated fatigue lifetimes are basically in an error factor of three.
(3) The presented critical plane determination approach can be combined with stress-based critical plane models to conduct fatigue life prediction, and predicted fatigue lives are mainly falling in an error factor of three for the investigated two materials.

Declaration of Competing Interest

The authors declare that they have no known competing financial interests or personal relationships that could have appeared to influence the work reported in this paper.

Acknowledgements

The present research is supported by the Academic Research Projects of Beijing Union University (No. ZK80202101), R & D Program of Beijing Municipal Education Commission (KM202211417012), National Natural Science Foundation of China (Nos. 12002186, 12072345, 12002185 and 51905334), Shanghai Sailing Program (19YF1418600), Science Center for Gas Turbine Project (P2022-B-III-008-001), and the Beijing Postdoctoral Research Foundation (2022-ZZ-044).

REFERENCES

[1] Liao D, Zhu SP, Qian G. Multiaxial fatigue analysis of notched components using combined critical plane and critical distance approach. Int J Mech Sci 2019;160:38–50.

[2] Zhu SP, Yu ZY, Correia J, De Jesus A, Berto F. Evaluation and comparison of critical plane criteria for multiaxial fatigue analysis of ductile and brittle materials. Int J Fatig 2018;112:279–88.
[3] Zhang ZL, Cheng Q, Qi BB, Tao ZQ. A general approach for the machining quality evaluation of S-shaped specimen based on POS-SQP algorithm and Monte Carlo method. J Manuf Syst 2021;60:553–68.
[4] Liu BW, Yan XQ. A new model of multiaxial fatigue life prediction with the influence of different mean stresses. Int J Damage Mech 2019;28(9):1323–43.
[5] Ahmadzadeh GR, Varvani-Farahani A. Energy-based damage descriptions to assess fatigue life of steel samples undergoing various multiaxial loading spectra. Int J Damage Mech 2019;28(1):35–57.
[6] Franko M, Sedlacek M, Podgornik B, Nagode M. Validation of linear damage rules using random loading. Int J Damage Mech 2017;26(3):463–79.
[7] Gorthofer J, Schneider M, Hrymak A, Bohlke T. A convex anisotropic damage model based on the compliance tensor. Int J Damage Mech 2022;31(1):43–86.
[8] Baranger E. Extension of a fourth-order damage theory to anisotropic history: application to ceramic matrix compostites under a multi-axial non-proportional loading. Int J Damage Mech 2018;27(2):238–52.
[9] Bannantine JA. A variable amplitude multiaxial fatigue life prediction method. PhD Thesis. University of Illinois at Urbana-Champaign; 1989.
[10] Socie DF. Multiaxial fatigue damage models. Journal of Engineering Materials and Technology, Transactions of the ASME. 1987;109(4):293–8.
[11] Ahmadzadeh GR, Varvani-Farahani A. Fatigue life assessment of steel samples under various multiaxial loading spectra by means of Smith-Watson-Topper type damage descriptions. Fatig Fract Eng Mater Struct 2018;41(7):1588–601.
[12] Smith KN, Watson P, Topper TH. Stress-strain function for the fatigue of metals. J Mater 1970;5(4):767–78.
[13] Fatemi A, Socie DF. A critical plane approach to multiaxial fatigue damage including out-of-plane loading. Fatig Fract Eng Mater Struct 1988;11(3):149–65.
[14] Wang CH, Brown MW. A path-independent parameter for fatigue under proportional and nonproportional loading. Fatig Fract Eng Mater Struct 1993;16(12):1285–98.
[15] Varvani-Farahani A. A new energy-critical plane parameter for fatigue life assessment of various metallic materials subjected to in-phase and out-of-phase multiaxial fatigue loading conditions. Int J Fatig 2000;22(4):295–305.
[16] Varvani-Farahani A, Kianoush MR, Sharma M. Fatigue failure assessment of engineering components under service loading conditions. Mater Des 2007;28(2):575–80.
[17] Kadhim NA, Mustafa M, Varvani-Farahani A. Fatigue life prediction of low-alloy steel samples undergoing uniaxial random block loading histories based on different energy-based damage descriptions. Fatig Fract Eng Mater Struct 2015;38(1):69–79.
[18] Lei BM, Tran VX, Taheri S, Roux JCI, Curtit F, He M, et al. Toward consistent fatigue crack initiation criteria for 304L austenitic stainless steel under multi-axial loads. Int J Fatig 2015;75:57–68.
[19] Wu ZR, Hu XT, Li ZX, Song YD. Evaluation of fatigue life for titanium alloy TC4 under variable amplitude multiaxial loading. Fatig Fract Eng Mater Struct 2015;38(4):402–9.
[20] Wang C, Shang DG, Wang XW, Chen H, Liu JZ. Comparison of HCF life prediction methods based on different critical planes under multiaxial variable amplitude loading. Fatig Fract Eng Mater Struct 2015;38(4):392–401.
[21] Wang YY, Susmel L. The Modified Manson–Coffin Curve Method to estimate fatigue lifetime under complex constant and variable amplitude multiaxial fatigue loading. Int J Fatig 2016;83:135–49.
[22] Araujo JA, Carpinteri A, Ronchei C, Spagnoli A, Vantadori S. An alternative definition of the shear stress amplitude based on the Maximum Rectangular Hull method and application to the C–S (Carpinteri–Spagnoli) criterion. Fatig Fract Eng Mater Struct 2014;37(7):764–71.
[23] Shamsaei N, Gladskyi M, Panasovskyi K, Shukaev S, Fatemi A. Multiaxial fatigue of titanium including step loading and load path alteration and sequence effects. Int J Fatig 2010;32(11):1862–74.
[24] Shamsaei N, Fatemi A, Socie DF. Multiaxial fatigue evaluation using discriminating strain paths. Int J Fatig 2011;33(4):597–609.
[25] Wang L, Wang DJ. Life prediction approach for random multiaxial fatigue. Chin J Mech Eng 2005;18(1):145–8.
[26] Carpinteri A, Spagnoli A, Vantadori S. Reformulation in the frequency domain of a critical plane-based multiaxial fatigue criterion. Int J Fatig 2014;67:55–61.
[27] Carpinteri A, Spagnoli A. Multiaxial high-cycle fatigue criterion for hard metals. Int J Fatig 2001;23:135–45.
[28] Fatemi A, Shamsaei N. Multiaxial fatigue: an overview and some approximation models for life estimation. Int J Fatig 2011;33(8):948–58.
[29] Tao ZQ, Shang DG, Liu H, Chen H. Life prediction based on weight-averaged maximum shear strain range plane under multiaxial variable amplitude loading. Fatig Fract Eng Mater Struct 2016;39:907–20.
[30] Macha E. Simulation investigations of the position of fatigue fracture plane in materials with biaxial loads. Int J Fatig 1989;20:153–63.
[31] Ahmadzadeh GR, Varvani-Farahani A. Fatigue damage and life evaluation of SS304 and Al 7050-T7541 alloys under various multiaxial strain paths by means of energy-based Fatigue damage models. Mech Mater 2016;98:59–70.
[32] Socie DF, Waill LA, Dittmer DF. In: Miller KJ, Brown MW, editors. Biaxial fatigue of Inconel 718 including mean stress effects, I multiaxial fatigue. Philadelphia: ASTM STP 853; 1985. p. 463–81.
[33] Ma S, Markert B, Yuan H. Multiaxial fatigue life assessment of sintered porous iron under proportional and non-proportional loadings. Int J Fatig 2017;97:214–26.
[34] Langlais TE, Vogel JH, Chase TR. Multiaxial cycle counting for critical plane methods. Int J Fatig 2003;25:641–7.
[35] Zhang JL, Shang DG, Sun YJ, Wang XW. Multiaxial high-cycle fatigue life prediction model based on the critical plane approach considering mean stress effects. Int J Damage Mech 2018;27(1):32–46.
[36] Wang XW, Shang DG, Sun YJ, Chen H. Multiaxial high-cycle fatigue life prediction model considering mean stress effects under constant and variable amplitude loading. Theor Appl Fract Mech 2018;96:676–87.
[37] Xia TX, Yao WX. Comparative research on the accumulative damage rules under multiaxial block loading spectrum for 2024-T4 aluminum alloy. Int J Fatig 2013;48:257–65.
[38] Deng QY, Zhu SP, He JC, Li XK, Carpinteri A. Multiaxial fatigue under variable amplitude loadings: review and solutions. International Journal of Structural Integrity 2022;13(3):349–93.
[39] Wang J, Liu J, Hua F, He Y, Wang X. Critical plane-based fatigue life model under multiaxial random loading. International Journal of Structural Integrity 2022;13(5):845–56.
[40] He Y, Liu J, Hua F, Zhao H, Wang. J. Low-cycle multiaxial random fatigue life prediction model based on equivalent

stress transformation. International Journal of Structural Integrity 2022;13(5):870–82.
[41] Ma M, Liu X. Multiaxial fatigue life prediction for metallic materials considering loading path and additional hardening effect. International Journal of Structural Integrity 2022;13(3):534–63.
[42] Correia JAFO, De Jesus AMP, Fernández-Canteli A, Calcada RAB. Modelling probabilistic fatigue crack propagation rates for a mild structural steel. Frat Ed Integrità Strutt 2015;31:80–96. https://doi.org/10.3221/IGF-ESIS.31.07.
[43] De Jesus AMP, Correia JAFO. Critical assessment of a local strain-based fatigue crack growth model using experimental data available for the P355NL1 steel. J Press Ves Technol 2013;135(1):011404.
[44] Liao D, Zhu SP, Correia JAFO, De Jesus AMP, Calcada R. Computational framework for multiaxial fatigue life prediction of compressor discs considering notch effects. Eng Fract Mech 2018;202:423–35. https://doi.org/10.1016/j.engfracmech.2018.08.009.
[45] Rozumek D, Marciniak Z. Fatigue crack growth in AlCu4Mg1 under nonproportional bending with torsion loading. Mater Sci 2011;46(5):685–94.
[46] Dantas R, Correia J, Lesiuk G, Rozumek D, Zhu S-P, de Jesus A, et al. Evaluation of multiaxial high-cycle fatigue criteria under proportional loading for S355 steel. Eng Fail Anal 2021;120:105037.
[47] Wang RZ, Gu HH, Zhu SP, Li KS, Wang J, Wang XW, et al. A data-driven roadmap for creep-fatigue reliability assessment and its implementation in low-pressure turbine disk at elevated temperatures. Reliab Eng Syst Saf 2022;225:108523.
[48] Sun L, Zhang XC, Wang RZ, Wang XW, Tu ST, Suzuki K, et al. Evaluation of fatigue and creep-fatigue damage levels on the basis of engineering damage mechanics approach. Int J Fatig 2022;166:107277.
[49] Li KS, Cheng LY, Xu Y, Wang RZ, Zhang Y, et al. A dual-scale modelling approach for creep-fatigue crack initiation life prediction of holed structure in a nickel-based superalloy. Int J Fatig 2022;154:106522.
[50] Li KS, Wang RZ, Yuan GJ, Zhu SP, Zhang XC, Tu ST, et al . A crystal plasticity-based approach for creep-fatigue life prediction and damage evaluation in a nickel-based superalloy. Int J Fatig 2021;143:106031.
[51] Cheng LY, Wang RZ, Wang J, Zhu SP, Zhao PC, Miura H, et al. Cycle-dependent creep-fatigue deformation and life predictions in a nickel-based superalloy at elevated temperature. Int J Mech Sci 2021;206:106628.
[52] Wang RZ, Cheng LY, Zhu SP, Zhao PC, Miura H, Zhang XC, et al. Semi-quantitative creep-fatigue damage analysis based on diffraction-based misorientation mapping and the correlation to macroscopic damage evolutions. Int J Fatig 2021;149:106227.